Drying Technology
An International Journal

ISSN: (Print) (Online) Journal homepage: www.tandfonline.com/journals/ldrt20

Understanding the operating limitations of an internal-mixing Air-Core-Liquid-Ring (ACLR) nozzle for process intensification in spray drying

Miguel Ángel Ballesteros Martínez & Volker Gaukel

To cite this article: Miguel Ángel Ballesteros Martínez & Volker Gaukel (13 Mar 2024): Understanding the operating limitations of an internal-mixing Air-Core-Liquid-Ring (ACLR) nozzle for process intensification in spray drying, Drying Technology, DOI: 10.1080/07373937.2024.2328300

To link to this article: https://doi.org/10.1080/07373937.2024.2328300

© 2024 The Author(s). Published with license by Taylor & Francis Group, LLC

Published online: 13 Mar 2024.

Submit your article to this journal

Article views: 221

View related articles

View Crossmark data

Full Terms & Conditions of access and use can be found at
https://www.tandfonline.com/action/journalInformation?journalCode=ldrt20

DRYING TECHNOLOGY
https://doi.org/10.1080/07373937.2024.2328300

Taylor & Francis
Taylor & Francis Group

OPEN ACCESS Check for updates

Understanding the operating limitations of an internal-mixing Air-Core-Liquid-Ring (ACLR) nozzle for process intensification in spray drying

Miguel Ángel Ballesteros Martínez and Volker Gaukel

Institute of Process Engineering in Life Sciences: Food Process Engineering, Karlsruhe Institute of Technology, Karlsruhe, Germany

ABSTRACT

Spray drying is a widely used method for producing food powders in large quantities, but it also has a high energy demand. To address this, researchers have long aimed to increase the solid content of liquid feeds, which poses the challenge of atomizing high-viscosity liquids into fine droplets. The Air-Core-Liquid-Ring (ACLR) nozzle offers a potential solution by inducing an internal annular flow, though it faces its own limitations due to internal flow instabilities. This study investigates how the nozzle flow conditions impact spray performance under different process conditions and liquid viscosities. We found that internal lamella thickness and atomization uniformity vary with pressure, viscosity, and liquid volume flow. Nonetheless, pressure appears to be the real critical factor in that case. The Air-to-Liquid Ratio (ALR) might be more decisive for the droplet size distribution than liquid viscosity. Future research should explore higher viscosities and consider simulations to circumvent experimental limitations.

ARTICLE HISTORY
Received 25 October 2023
Revised 12 January 2024
Accepted 5 March 2024

KEYWORDS
Spray drying; high viscosity; ACLR; internal-mixing nozzle; spray performance

Introduction

Liquid atomization has applications in many industrial processes, such as combustion, surface coatings, and spray drying. Its objective is to increase the surface area between the liquid phase that is being atomized and the surrounding gas, which promotes the rate of heat and mass transfer.[1] The enlargement of the surface area requires energy, which must be transferred to the liquid using a suitable atomizer,[2] for which there is a vast number of different types, each with their own strengths and weaknesses.

This particular study focused on understanding the behavior and performance of the Air-Core-Liquid-Ring (ACLR) nozzle,[3] which is a type of internal-mixing pneumatic nozzle. A schematic of the ACLR-nozzle is shown in Figure 1. The device is composed of two concentric tubes. The outer casing is where the liquid feed flows, while a capillary at the center carries the compressed air and injects it at the core of the liquid phase in a mixing chamber. This favors the formation of an annular flow, with a liquid lamella (or ring) around the air core. As this two-phase flow exits the nozzle, the air phase expands, and the liquid film forms a cone that breaks up into droplets.[4]

The two-phase flow inside the atomizer allows it to handle liquids with higher viscosities than pressure swirl nozzles.[3] Additionally, because the gas and liquid flows are combined inside the nozzle,[5] lower gas flow rates are possible in internal-mixing atomizers than in external-mixing atomizers.[6] The ability to handle higher viscosities makes the ACLR-nozzle of special importance for spray drying, since it also means that higher solid concentrations can be handled.[7] Based on a model calculation by Fox et al.,[8] Wittner et al.[9] estimated that the ACLR-nozzle can potentially reduce total energy consumption in a spray-drying process up to 29% compared to a process using a standard pressure swirl nozzle.

However, while the need to atomize more viscous feeds has been already identified, the range of viscosities that has been successfully atomized is limited. Wittner et al.[9] reported viscosities, using maltodextrin solutions, of up to 390 mPas and a dry-matter content of 47%. Yu et al.[10] reported viscosities, using domestic sludges, of barely 26 mPa.s and a dry-matter content of 15%. It is clear that to maximize energy savings, the maximum range of atomizable viscosities still needs to be identified. However, that first requires determining

CONTACT Miguel Ángel Ballesteros Martínez miguel.ballesteros@kit.edu Institute of Process Engineering in Life Sciences: Food Process Engineering, Karlsruhe Institute of Technology, Kaiserstraße 12, 76131 Karlsruhe, Germany.

© 2024 The Author(s). Published with license by Taylor & Francis Group, LLC
This is an Open Access article distributed under the terms of the Creative Commons Attribution License (http://creativecommons.org/licenses/by/4.0/), which permits unrestricted use, distribution, and reproduction in any medium, provided the original work is properly cited. The terms on which this article has been published allow the posting of the Accepted Manuscript in a repository by the author(s) or with their consent.

which performance parameters are affected the most by the feed viscosity.

Stähle et al.[3] and Wittner et al.[11] already analyzed how the viscosity affected the Sauter mean diameter and its temporal stability. Additionally, Wittner et al.[11] identified that a higher viscosity increases the variation in the lamella thickness inside the nozzle, which leads to the higher instability in the Droplet Size Distribution (DSD), although they only analyzed two different viscosities. Based on these previous results, this study focused on how a wide range of liquid viscosities and operating conditions affect the internal flow instabilities of the nozzle and how these instabilities relate to the spray uniformity, i.e. the DSD width and modality, and the spray angle, which had not so far been considered as performance parameters.

While we performed the analysis with experimental measurements, we also adapted a CFD model from a previous study[12] to simulate the external flow near the outside of the nozzle. This included expanding the simulated volume two half of the nozzle instead of the original quarter, and adding a region of air (which we denote as airbox) at the exit of the nozzle. This complementary analysis had two main future objectives. On the one hand, it allows us to evaluate liquid viscosities and operating conditions beyond the restrictions and limitations of our experimental setup. On the other hand, CFD modeling provides a deeper insight into the fluid mechanics at play during the atomization because it can determine flow characteristics that are not measurable experimentally, such as velocity profiles or 3D reconstructions of the spray cone.

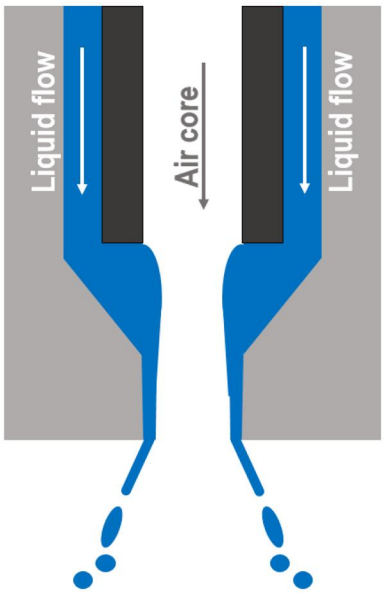

Figure 1. Schematic of the Air-Core-Liquid-Ring (ACLR) atomizer. Taken from Ballesteros Martínez and Gaukel.[12]

Experimental setup

Model solutions

Experiments were carried out with water and maltodextrin solutions. Table 1 shows the different types of maltodextrin (Cargill Deutschland GmbH, Düsseldorf, Germany), and the concentrations used to achieve the range of viscosities that we investigated. The fluid properties of these model solutions were also introduced into the simulations (see Table 1), so that they were comparable to the experimental results. The properties of air and water were taken from the database of Siemens AG.[13] The viscosity of the maltodextrin solution was measured with a rotational rheometer (Physica MCR 301, Geometry DG26.7, Anton Paar, Graz, Austria) at shear rates between 1 to 10^3 s^{-1}. The solution density was measured by use of a 25 cm^3 pycnometer (Blaubrand, Brand, Wertheim, Germany).

Spray test rig and spray characterization

All experiments were carried out in a spray test rig, which has been described in detail in previous studies.[11,12] In short, it is composed of a closed cabin with a vertical atomizer on top. The liquid flow is supplied by an eccentric screw pump (NM011BY, Erich Netzsch GmbH and Co. Holding KG, Waldkraiburg, Germany) and measured by a gear flow meter (VSI 044/16, VSE GmbH, Neuenrade, Germany). Air is supplied by a compressor (Renner RSF-Top 7.5, Renner GmbH, Güglingen, Germany). The air pressure is adjusted with a pressure regulator, and its resulting volume flow is measured by a gas flow meter (ifm SD6000, ifm electronic, Essen, Germany).

The outer casing of the ACLR was constructed with clear acrylic. This allowed the direct optical visualization of the flow conditions inside the atomizer using a high-speed video camera (OS3-V3-S3, Integrated Design Tools Inc., Tallahassee, FL, USA) and a high-performance light-emitting diode system

Table 1. Properties of model solutions used.

Maltodextrin	Mass fraction/% wt.	Viscosity/ mPa·s	Density/ $kg \cdot m^{-3}$
C*DryTM MD 01910 (DE 13.9)	25.5	9	1090
	45	105	1208
	47	140	1211
C*DryTM MD 01958 (DE 8.8)	45	225	1211
	47	340	1234

(constellation 120 E, ImagingSolution GmbH, Eningen unter Achalm, Germany). The camera recorded the internal flow at a framerate of 20 kHz. Each measurement was composed of 10,000 images, which amounts of 0.5 s measurement time. The exposure time of each image was 5 µs, and the resolution was around 10 µm/pixel. The images were processed with a Matlab (The MathWorks Inc., Natick, MA, USA) code to measure the thickness of the liquid film, i.e. lamella, inside the nozzle. The algorithm of the code is described in detail in Wittner et al..[11] To statistically characterize the lamella thickness variation, the 5%, 50% and 95% percentiles, which are denoted as $h_{5,0}$, $h_{50,0}$, and $h_{95,0}$, respectively, were calculated for each combination of pressure and viscosity. Additionally, a set of five random recorded images was also picked to manually determine an average spray angle.

Droplet size measurements were performed using a laser diffraction spectroscope (Spraytec, Malvern Instruments, Malvern, UK). It was equipped with a 750 mm focal lens, offering a droplet size measuring range of 2–2000 µm. The spectrometer was placed 250 mm underneath the exit orifice of the atomizer. The laser beam crossed the full cone spray angle at the nozzle axis centerline. Measurements were conducted over a time of 30 s, leading to a time-averaged distribution of the droplet size. To statistically characterize the atomization uniformity, the 10% and 90% percentiles, which are denoted as $x_{10,3}$ and $x_{90,3}$, respectively, were calculated for each pressure and viscosity. The difference between the two percentiles was defined as the distribution range.

Numerical modeling

The CFD model, including the physics models and the mesh, was adapted in STAR-CCM + v.2206 (Siemens AG, Munich, Germany), from our previous work,[12] which had been implemented in ANSYS Fluent 2019 R3 (Ansys, Inc., Canonsburg, Pennsylvania, USA). The multiphase flow that develops in the nozzle was modeled as an immiscible mixture of two phases: The liquid phase was set as incompressible and Newtonian, while the gas phase was assumed as ideal and Newtonian.

Governing equations

The multiphase flow was simulated using the Volume-Of-Fluid method. This model assumes that all fluid phases share the same pressure and velocity fields. This means that the two-phase system is modeled as a single-phase fluid, whose physical properties are calculated from the volume averages of the properties of the actual phases.[14] This means that only one momentum equation, like the one shown in Equation (1), is solved to predict the velocity and pressure fields of the mixture.

$$\frac{\mathrm{d}}{\mathrm{d}t}\int_V \rho\mathbf{u}\mathrm{d}V+\int_A \rho\mathbf{u}\times\mathbf{u}\mathrm{d}A=-\int_A p\mathbf{I}\cdot\mathrm{d}A+\int_A \boldsymbol{\tau}\cdot\mathrm{d}A+\int_V \mathbf{f_b}\mathrm{d}V \tag{1}$$

On the left side of the equation are the terms for transient and convective transport. $\mathbf{u}$ is the velocity, while ρ represents the volume-averaged density. On the right side of the equation are the pressure gradient term, the viscous stress term, and external force term. Correspondingly, p is the pressure, $\boldsymbol{\tau}$ is the stress tensor, and $\mathbf{f_b}$ is the external body force vector. It should be noted that $\mathbf{I}$ is the identity matrix.[15] As for the integrals, V represents the volume; conversely, $\boldsymbol{A}$ is the normal vector of the surface area. Finally, t is the time.

Using the VOF formulation, the internal flow was modeled as transient because of the unstable free surface between the phases. Additionally, to account for turbulence, an appropriate Reynolds-Averaged (RANS) model was chosen, namely, the k-ω SST. This model was selected after comparing with other RANS models, namely k-ε and RSM, and evaluating how they captured the flow instabilities that occur inside of the nozzle. More information about the model selection can be found in Ballesteros Martinez & Gaukel.[12] In summary, the k-ω SST model reported the best balance between accuracy and computational efficiency. Additional information about the equations that compose this model and how they are implemented into the governing equations is presented in Baker et al.[16]

Mesh generation

The mesh configuration and density was based on the mesh independence analysis done on our previous study, which was performed for a quarter of a nozzle.[12] More information about the mesh specifics and the results of the mesh independence test can be found there. The resulting the mesh utilized is shown in Figure 2. It should be noted that the nozzle geometry and design was, in principle, the same as the one in the previous work. However, for this study, the simulated volume was doubled to half a nozzle, to get a better visualization of the spray cone. Additionally, for the same purpose, an airbox was added

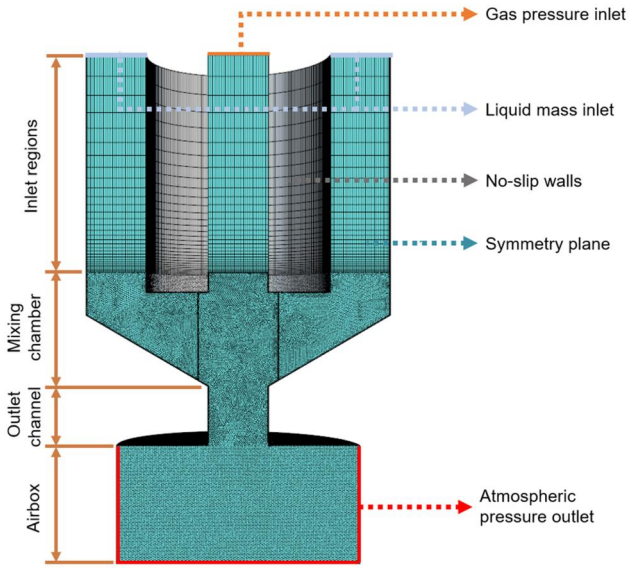

Figure 2. Simulated mesh of the ACLR atomizer. Half of the nozzle was simulated along with an airbox underneath the nozzle exit. The inlet regions were meshed with hexahedral cells, while a finer polyhedral mesh was utilized for the other sections of the simulated volume. The boundary conditions are also indicated.

underneath the nozzle exit, with a height of two times the outlet diameter (D) and a width of 4D. The airbox was meshed with the same cell size and cell type as the one used for the outlet diameter.

Boundary and simulating conditions

The boundary conditions set for the simulation are shown in Figure 2. Just as in the experimental setup, the gas pressure and the liquid flowrate were the inlet boundary conditions set in the simulations. On the other hand, the exit of the simulated volume was set as an atmospheric pressure outlet. Because only half the nozzle was simulated, a symmetry plane was also implemented. All simulations were run for at least 8 ms. we accounted for 4 ms of initialization time and used the other 4 ms of simulated time for the time-dependent and time-averaged analysis. An adaptative timestep was therefore introduced to better capture the flow variations. This ensured that the local CFL number across all the cells of the mixing chamber and outlet channel was always below one.

Model validation

The numerical model has already been validated with experimental results with viscosities of up to 140 mPa·s. It can predict the average lamella thickness and the operating ALR, both with a relative error of around 10%.[12] Since the previous model had only been validated with the internal flow variation, a secondary validation was performed here using the spray angle, to ensure that the model could also reasonably capture the external flow of the liquid after the nozzle exit. The spray angle in the simulation was determined by hand following the same procedure as with the experiments, although the measurement was performed without repetitions in this case.

Results and discussion

Effect of viscosity on internal flow stability

Wittner et al.[11] already indicated that increasing viscosities have a negative effect on the internal flow stability, while increasing Air-to-Liquid Ratios (ALRs) have a positive effect on it. Nevertheless, we wanted to understand how the two factors (i.e. ALR and viscosity) interact. For that reason, we measured the lamella thickness for a wide range of liquid viscosities, at three different pressures and two different liquid volume flows. Both the volume flow and the air pressure were taken into consideration because they determine the ALR and can be easily set with the experimental setup.

To evidence the flow instabilities, the percentiles $h_{5,0}$, $h_{50,0}$, and $h_{95,0}$ of the lamella thickness measurements are plotted for each viscosity, which is shown in Figure 3. The shaded region highlights then the range of lamella thicknesses that can be expected at a specific pressure and viscosity. For the higher liquid volume flow of 40 L·h^{-1}, an additional pressure of 0.7 MPa was evaluated. As expected, the $h_{50,0}$ and $h_{95,0}$ tend to increase with viscosity. In comparison, the $h_{5,0}$ remains relatively constant with changes in liquid viscosities and operating conditions. It is interesting to note that the increase for the $h_{95,0}$ is smaller at higher pressures. In contrast, the $h_{50,0}$ is shifted downwards as pressure increases, but its increase with viscosity does not diminish with higher pressures, Looking at the liquid volume flow, a lower volume flow also causes the percentiles to increase less with viscosity, though, in this case, the $h_{50,0}$ seems to be more affected than the $h_{95,0}$. The behavior of the $h_{50,0}$ is severely flattened with a lower liquid volume flow; the $h_{95,0}$ maintains comparatively the same behavior as with 40 L·h^{-1}, even if the increase rate is slightly dampened. This means that the general behavior of the flow variations follows what is expected from previous studies,[3,4] since they decrease with higher pressures and lower liquid volume flows, which are both related to higher ALRs.

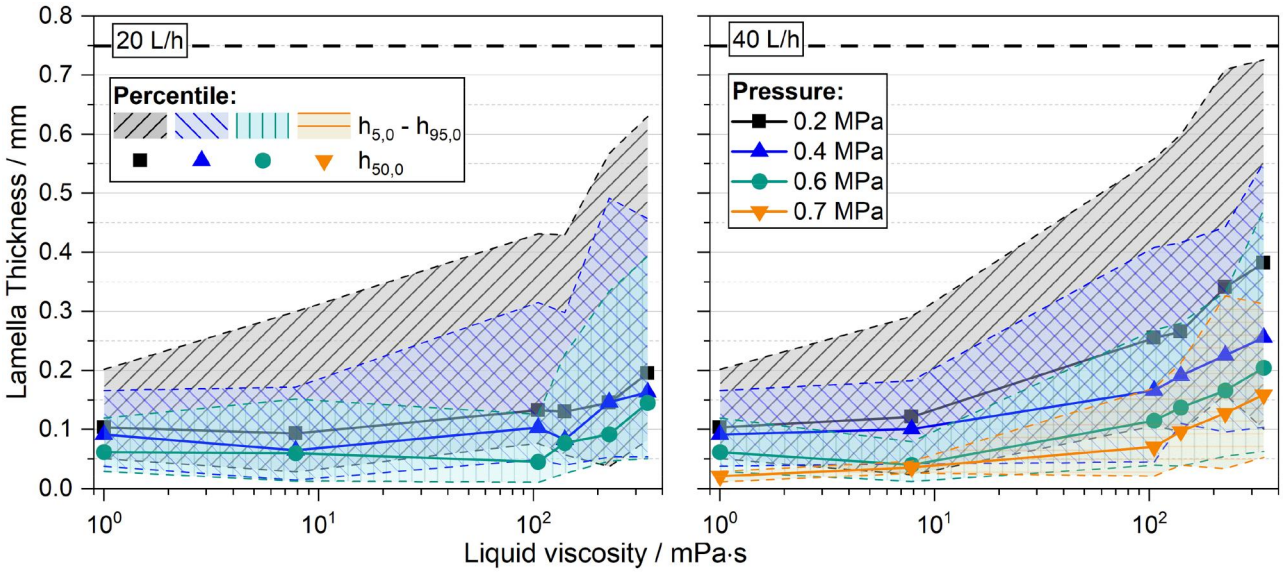

Figure 3. Lamella thickness for maltodextrin solutions of increasing viscosities at different gas pressures (indicated with the different colors and markers) and two different liquid volume flows (Left: 20 L·h^{-1}; Right: 40 L·h^{-1}). For both left and right graphs, the median ($h_{50,0}$) is indicated by the marker. The 5% and 95% percentiles ($h_{5,0}$ and $h_{95,0}$) are indicated as the shaded regions, showing the variation range of the thickness. The black dashed line represents the radius of the outlet channel; a lamella thickness of this magnitude would mean that the whole nozzle is filled with liquid.

As the top percentile, it would be expected that the $h_{95,0}$ is more sensitive to all changes in process parameters. This is, however, not always the case, as it seen with the liquid volume flow. Nonetheless, it is still clear that the quasi-exponential increase of the characteristic values at higher viscosities, especially of the $h_{95,0}$, is the limiting operability factor for the atomization. Future investigations with higher viscosities might show the upper limit of viscosity that allows a stable atomization. Since the experimental setup is limited to gas pressures of up to 0.7 MPa, these investigations might have to be complemented with numerical simulations of the nozzle to evaluate higher operating pressures.

Effect of viscosity on spray performance

As first recognized by Wittner et al.,[4] the internal flow instabilities have a negative effect on the DSD, which is one of our key spray performance parameters. With that in mind, we measured the cumulative volumetric DSD for two of the highest viscosities analyzed in the previous section (140 and 340 mPa·s). This analysis was performed at the same three pressures and two liquid volume flows and is shown in Figure 4. The characteristic values of the DSD (the $x_{10,3}$, $x_{50,3}$, and $x_{90,3}$ percentiles) all decrease with pressure and increase with viscosity, as well as with liquid volume flow. For clarification, to see how a percentiles changes (e.g. $x_{50,3}$), one can focus on the corresponding ordinate in the y-axis (which in the example would be 0.5) and follow the horizontal line that intersects the DSDs. It is fairly evident then that any increase in the ALR leads to smaller values in the corresponding percentile. This correlates with the behavior observed for the internal lamella thickness. This correlation also agrees with the behavior observed by Wittner et al.[4] and Stähle et al.,[3] although they focused rather on the Sauter mean diameter and its temporal stability.

However, not only is the temporal stability important for process design, the atomization uniformity must also be considered. In this study, atomization uniformity refers to the size uniformity of the droplets after atomization,[17] which we evaluated using two criteria. On one side, we evaluated qualitatively the unimodality of the DSDs that are plotted in Figure 4. In doing so, one can notice that, for both viscosities, increasing pressure and lowering the volume flow (meaning increasing the ALR) shifts the DSD to smaller values and turns it from multimodal to unimodal. A higher viscosity seems to diminish the amount shift on the DSD caused by the ALR. This correlates to the behavior of the lamella thickness shown in Figure 3. As the viscosity increases, higher pressures are required to keep the same internal flow variation, exemplified by width of the shaded region in Figure 3.

As a side note, the amount of overlap that seems to occur between the DSD at different operating conditions is interesting. This is related to the ALR, which

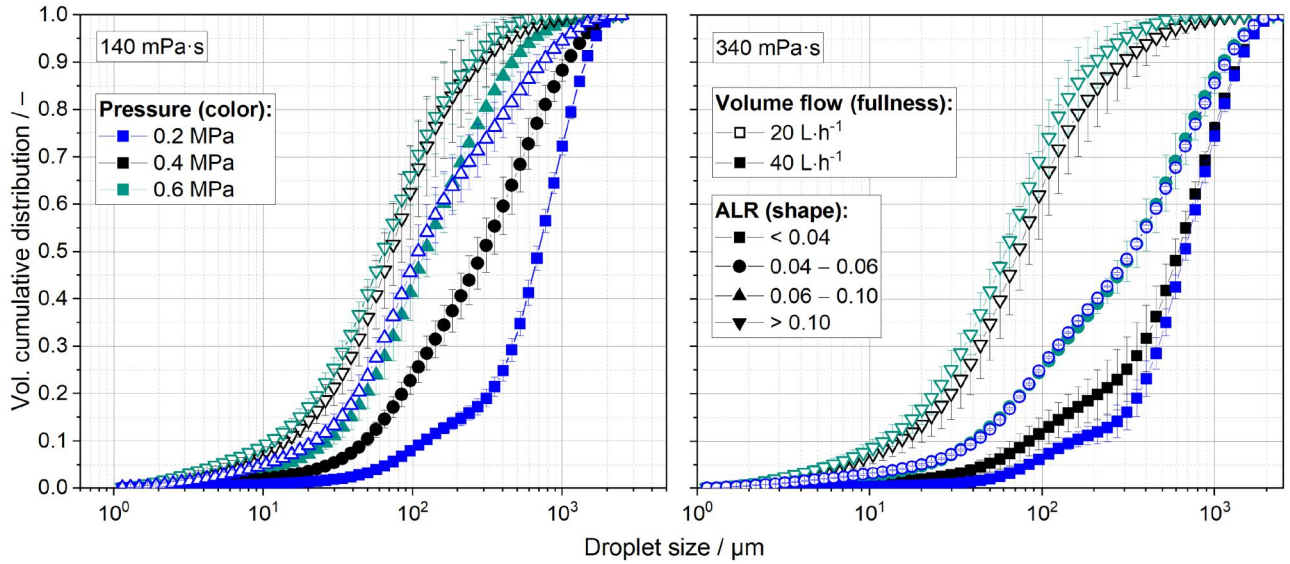

Figure 4. Droplet size distribution of maltodextrin solutions of two different viscosities (Left: 140 mPa·s; Right: 340 mPa·s,), atomized at different gas pressures (indicated with line and marker color) with two different liquid volume flows (marked with either filled or empty markers). The ALR of each distribution are classified into four ranges, each marked with a different marker shape. The error bars also indicated for each distribution.

Table 2. Range and uniformity of the DSD for different pressures and viscosities.

Volume flow/L·h^{-1}	Pressure/MPa	Range/µm†		ALR/-	
		140 mPa·s	340 mPa·s	140 mPa·s	340 mPa·s
20	0.2	1127 ± 6	865 ± 298	0.068^{C}	0.048^{B}
	0.4	268 ± 128	278 ± 121	0.136^{D}	0.099^{D}
	0.6	231 ± 87	191 ± 71	0.214^{D}	0.150^{D}
40	0.2	1311 ± 28	1232 ± 48	0.023^{A}	0.018^{A}
	0.4	1015 ± 97	1284 ± 30	0.052^{B}	0.038^{A}
	0.6	437 ± 66	1078 ± 119	0.090^{C}	0.062^{B}

†Three replicate measurements were performed for each pressure.
ABCD The different ALR values were classified into four groups (A-D) based on the ranges described above in the text.

is known to be an important process parameter for the DSD with this type of nozzle.[3] To consider the effect of this parameter, we calculated the ALR for the different DSDs plotted in Figure 4. This is shown in Table 2 along with the range of the DSD, which is our second criterion of atomization uniformity. Coming back to the ALR, while the overlapping DSD do not share the same ALR, their ALR seems to fall within a same range, irrespective of the liquid viscosity. ALRs under 0.04 (marked with A in Table 2) lead to similar multimodal DSD with a large portion of large droplets. ALRs between 0.04 and 0.06 (marked with B) present a DSD with less multimodality but still a large portion of large droplets. ALRs from 0.06 to 0.1 (marked with C) transition to a unimodal DSD, which seems to converge to a final stable distribution for ALRs above 0.1 (marked with D). A next step would be to evaluate whether this convergence happens as well with higher viscosities, and whether there is a critical ALR that ensures this convergence irrespective of viscosity.

The range of the DSD (see Table 2) follows the same pattern as the characteristic values of the DSD. This is evidenced by its tendency to decrease with pressure and increase with volume flow, that means, it decreases with higher ALRs. The effect of the viscosity is not as clear. Under constant operating conditions, a higher viscosity does lead to a smaller ALR, because of the thicker liquid lamella; however, the effect of this is not evident on the droplet size range. The variation caused seems to be relatively small, so it is possible that a stronger tendency could be noticed when evaluating higher viscosities.

Simulation of external flow

Both the analysis of the internal flow and the DSD indicate that higher viscosities have to be evaluated. However, both highlight the limitation of expanding this analysis with the experimental setup: Higher viscosities require higher pressures to ensure internal flow stability and a unimodal DSD. These pressure requirements may quickly exceed the capability of our, or any, experimental setup, which is why we decided to utilize a CFD model. In that way, we should be able to evaluate any useful process condition without limitations of the experimental setup.

The results of this validation are shown in Table 3. The spray angle at three pressures was determined experimentally and with the simulation, for two

different viscosities: 8 and 140 mPa·s. Both in simulations and experiments, increasing the pressure or lowering the viscosity cause a wider spray cone (a larger spray angle), which makes sense since both are related to a thinner liquid lamella. Comparing between simulations and experiments, there seems to be in general a good agreement, considering the case at 0.6 MPa and 140 mPa·s as an outlier. As a side note, one can also notice that the variation of the spray angle, which is in general minor, does not change with pressure or viscosity, which is a good indicator for applications with larger viscosities. Further measurements that evaluate the temporal instability of the spray angle may confirm this.

Apart from the ability to simulate operating conditions beyond the limitations of the experimental setup, a CFD of the system also allows visualizing flow information that is not experimentally attainable. Figure 5 shows an example of this possible application, in that the spray cone at the nozzle exit was recreated. While in experiments, the 2D recordings are limited by the camera resolution and obscured by the spray mist, a simulation can accomplish full 3D reconstructions of the breakup of the liquid lamella. In the same way, extensive information can be obtained about other flow variables, e.g. the velocity or pressure drop.

Table 3. Spray angle in simulations (SIM) and experiments (EXP) for different pressures and viscosities. All spray angles were determined for a liquid flowrate of 40 L·h^{-1}.

	Spray angle[a]			
	8 mPa·s		140 mPa·s	
Pressure/MPa	EXP	SIM	EXP	SIM
0.2	41 ± 4°	44°	35 ± 6°	42°
0.4	56 ± 2°	58°	44 ± 4°	45°
0.6	70 ± 4°	70°	51 ± 4°	67°

[a]Measurement repeated five times in experiments, but no repetitions in simulations.

Conclusions

The correlation between internal and external flow stability of the ACLR nozzle was studied for viscosities up to 340 mPa·s. The variations in the internal lamella thickness behaved as expected, as it decreased with ALR and increased with viscosity. It was interesting to note that the two main characteristic values of the flow variations (the $h_{50,0}$ and $h_{95,0}$ of the lamella thickness) had different sensitivities to changes in liquid viscosity and operating conditions: The $h_{50,0}$ was more sensitive to changes in liquid volume flow, while the $h_{95,0}$ seemed to be more sensitive to changes in pressure. In fact, the pressure seems to be the limiting operating factor for the internal stability, since it is what most directly affects the $h_{95,0}$. This means that, as viscosity increases, a higher operating pressure is critical to ensure stable operation.

In regard to the characteristic values and range of the DSD, they followed the same behavior as the internal lamella thickness, which happened as expected. In the same way that, at increasing viscosities, a higher pressure is needed to keep the same $h_{95,0}$ of the lamella thickness, a higher pressure is also required to ensure a unimodal DSD with a small fraction of large droplets. Above a critical ALR of around 0.1, the DSD might converge to a final distribution

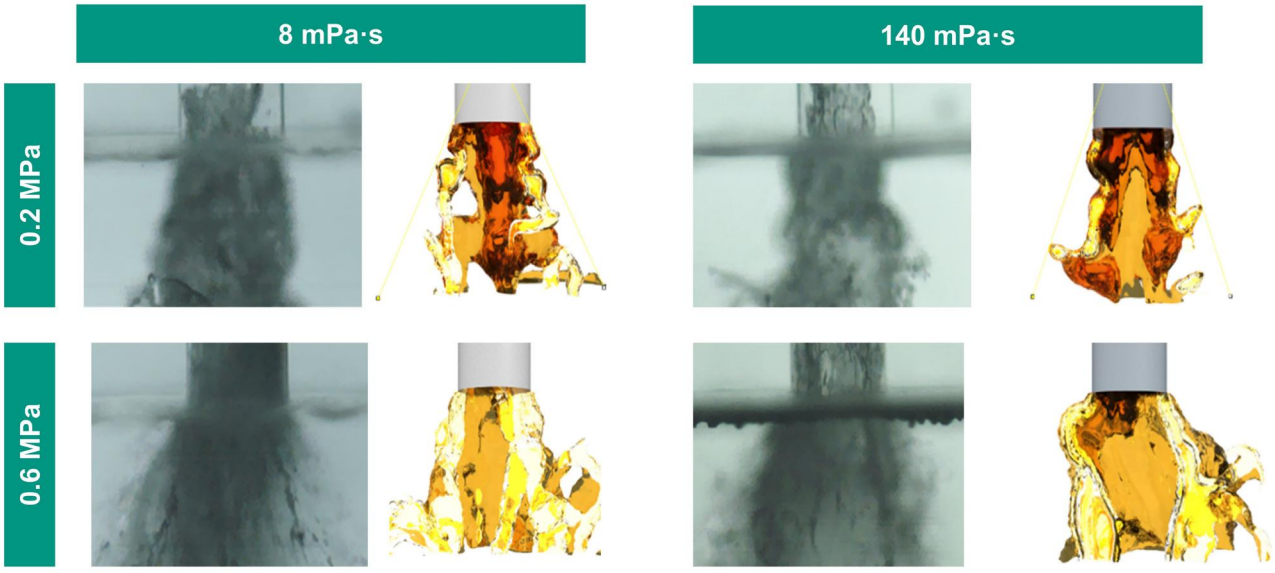

Figure 5. Experimentally observed spray cone (left) and simulated 3D-reconstruction of the liquid lamella (right) at the nozzle exit, for maltodextrin solutions of 8 and 140 mPa·s, at different pressures and a liquid flowrate of 40 L·h^{-1}.

irrespective of viscosity. This, however, will have to be investigated further with higher viscosities.

Both the analysis of the internal flow instability and of the DSD lead to the same conclusion: stable spraying with higher viscosities needs higher operating pressures. This means that simulations will have to complement the experimental measurements to evaluate until which point a stable atomization is possible. The validation of an existing CFD model with the spray angle provided promising results. In both experiments and simulations, the same trend was observed, as the spray cone widens with higher ALRs and smaller viscosities. The ability to obtain flow information that is not experimentally attainable is certainly one of the most alluring advantages of utilizing CFD simulations.

Acknowledgements

The researchers would like to thank Deisy Becerra for her aid in carrying out some of the experimental measurements, as well as the support by the state of Baden-Württemberg through access to the bwHPC.

Disclosure statement

The authors report there are no competing interests to declare.

Funding

This work was partly funded by the Deutsche Akademische Austauschdienst (DAAD), through one of their research grants for doctoral programs in Germany. The authors also acknowledge the financial support of the International Fine Particle Research Institute (IFPRI) and of the Kompetenznetz Verfahrenstechnik Pro3 e.V.

References

[1] Lee, K.; Abraham, J. Spray Applications in Internal Combustion Engines. In *Handbook of Atomization and Sprays: Theory and Applications*; Ashgriz, N., Ed.; Springer Science + Business Media LLC: Boston, MA, **2011**; pp 777–810.

[2] Lefebvre, A. H.; McDonell, V. G. *Atomization and Sprays*; CRC Press: Boca Raton, London, New York, **2017**.

[3] Stähle, P.; Gaukel, V.; Schuchmann, H. P. Comparison of an Effervescent Nozzle and a Proposed Air-Core-Liquid-Ring (ACLR) Nozzle for Atomization of Viscous Food Liquids at Low Air Consumption. *J. Food Process Engineering* **2017**, *40*, e12268. DOI: 10.1111/jfpe.12268.

[4] Wittner, M. O.; Karbstein, H. P.; Gaukel, V. Spray Performance and Steadiness of an Effervescent Atomizer and an Air-Core-Liquid-Ring Atomizer for Application in Spray Drying Processes of Highly Concentrated Feeds. *Chemical Engineering and Processing - Process Intensification* **2018**, *128*, 96–102. DOI: 10.1016/j.cep.2018.04.017.

[5] Wozniak, G. Technische Zerstäuber. In *Zerstäubungstechnik*; Wozniak, G., Ed.; Springer Berlin Heidelberg: Berlin, Heidelberg, **2003**; pp 57–87.

[6] Hammad, F. A.; Sun, K.; Jedelsky, J.; Wang, T. The Effect of Geometrical, Operational, Mixing Methods, and Rheological Parameters on Discharge Coefficients of Internal-Mixing Twin-Fluid Atomizers. *Processes* **2020**, *8*, 563. DOI: 10.3390/pr8050563.

[7] Rao, M. A. *Rheology of Fluid, Semisolid, and Solid Foods: Principles and Applications*, 3rd ed.; Springer: Boston, MA, **2014**.

[8] Fox, M.; Akkerman, C.; Straatsma, H.; de Jong, P. Energy Reduction by High Dry Matter Concentration and Drying. *New Food* **2010**, *6*, 60–62.

[9] Wittner, M. O.; Karbstein, H. P.; Gaukel, V. Energy Efficient Spray Drying by Increased Feed Dry Matter Content: Investigations on the Applicability of Air-Core-Liquid-Ring Atomization on Pilot Scale. *Drying Technol.* **2020**, *38*, 1323–1331. DOI: 10.1080/07373937.2019.1635616.

[10] Yu, C.; Cui, Y.; Liu, B.; Li, Y.; Wang, R.; He, C.; Li, J.; He, Q. Industrial-Scale Experimental Study of Internal-Mixing Air-Blast Nozzle for Sludge Atomization. *Drying Technol.* **2023**, *41*, 2281–2296. DOI: 10.1080/07373937.2023.2235412.

[11] Wittner, M.O.; Ballesteros, M.A.; Link, F.J.; Karbstein, H.P.; Gaukel, V. Air-Core–Liquid-Ring (ACLR) Atomization Part II: Influence of Process Parameters on the Stability of Internal Liquid Film Thickness and Resulting Spray Droplet Sizes. *Processes* **2019**, *7*(9), 616. DOI: 10.3390/pr7090616.

[12] Ballesteros Martínez, M. Á.; Gaukel, V. Time-Averaged Analysis and Numerical Modelling of the Behavior of the Multiphase Flow and Liquid Lamella Thickness inside an Internal-Mixing ACLR Nozzle. *Flow. Turbulence Combust.* **2023**, *110*, 601–628. DOI: 10.1007/s10494-023-00406-5.

[13] Siemens Industries Digital Software. Simcenter STAR-CCM + User Guide, Version 2206. **2022**. https://plm.sw.siemens.com/en-US/simcenter/fluids-thermal-simulation/star-ccm/

[14] Sun, S.; Zhang, T. Review of Classical Reservoir Simulation. In *Reservoir Simulations*; Elsevier: Amsterdam, **2020**; pp 23–86.

[15] Alizadeh Kaklar, Z.; Ansari, M. R. Numerical Analysis of the Internal Flow and the Mixing Chamber Length Effects on the Liquid Film Thickness Exiting from the Effervescent Atomizer. *J. Therm. Anal. Calorim.* **2019**, *135*, 1881–1890. DOI: 10.1007/s10973-018-7485-3.

[16] Baker, C.; Johnson, T.; Flynn, D.; Hemida, H.; Quinn, A.; Soper, D.; Sterling, M. *Train Aerodynamics*; Butterworth-Heinemann: Oxford, **2019**.

[17] Fan, S.; Chen, S.; Wu, Z.; Wu, S.; Chen, Y.; Liu, D.; Yao, Y.; Huang, J. Analysis of Droplet Size Distribution and Selection of Spray Parameters Based on the Fractal Theory. *J. Cleaner Prod.* **2022**, *371*, 133315. DOI: 10.1016/j.jclepro.2022.133315.